Astronomy
&
Astrophysics

Populations III.1 and III.2 gamma-ray bursts: constraints on the event rate for future radio and X-ray surveys

R. S. de Souza[1,2], N. Yoshida[1], and K. Ioka[3]

[1] IAG, Universidade de São Paulo, Rua do Matão 1226, Cidade Universitária, CEP 05508-900, São Paulo, SP, Brazil

[2] Institute for the Physics and Mathematics of the Universe, Todai Institutes for Advanced Study, University of Tokyo, 5-1-5 Kashiwanoha, Kashiwa, Chiba 277-8583, Japan
e-mail: rafael.desouza@ipmu.jp

[3] KEK Theory Center and the Graduate University for Advanced Studies (Sokendai), Tsukuba 305-0801, Japan

ABSTRACT

Aims. We calculate the theoretical event rate of gamma-ray bursts (GRBs) from the collapse of massive first-generation (Population III; Pop III) stars. The Pop III GRBs could be super-energetic with the isotropic energy up to $E_{iso} \gtrsim 10^{55-57}$ erg, providing a unique probe of the high-redshift Universe.

Methods. We consider both the so-called Pop III.1 stars (primordial) and Pop III.2 stars (primordial but affected by radiation from other stars). We employ a semi-analytical approach that considers inhomogeneous hydrogen reionization and chemical evolution of the intergalactic medium.

Results. We show that Pop III.2 GRBs occur more than 100 times more frequently than Pop III.1 GRBs, and thus should be suitable targets for future GRB missions. Interestingly, our optimistic model predicts an event rate that is already constrained by the current radio transient searches. We expect $\sim 10-10^4$ radio afterglows above ~ 0.3 mJy on the sky with ~ 1 year variability and mostly without GRBs (orphans), which are detectable by ALMA, EVLA, LOFAR, and SKA, while we expect to observe maximum of $N < 20$ GRBs per year integrated over at $z > 6$ for Pop III.2 and $N < 0.08$ per year integrated over at $z > 10$ for Pop III.1 with EXIST, and $N < 0.2$ for Pop III.2 GRBs per year integrated over at $z > 6$ with *Swift*.

Key words. stars: Population III – gamma-ray burst: general – radio lines: general – X-rays: general

1. Introduction

The first stars in the Universe are thought to have played a crucial role in the early cosmic evolution by emitting the first light and producing the first heavy elements (Bromm et al. 2009). Theoretical studies based on the standard cosmological model predict that the first stars were formed when the age of the Universe was less than a few hundred million years and that they were predominantly massive (Abel et al. 2002; Omukai & Palla 2003; Yoshida et al. 2006). Although there are a few observational ways to probe the early stellar populations, there has not yet been any direct observations of the so-called Population III (Pop III) stars.

Recently, it has been proposed that massive Pop III stars may produce collapsar gamma-ray bursts (GRBs), whose total isotropic energy could be $E_{iso} \gtrsim 10^{55-57}$ erg, i.e., $\gtrsim 2$ orders of magnitude above average (Komissarov & Barkov 2010; Toma et al. 2011; Mészáros & Rees 2010; Barkov 2010; Suwa & Ioka 2011). Even if the Pop III star has a supergiant hydrogen envelope, the GRB jet can break out the first star because of the longlasting accretion of the envelope itself (Suwa & Ioka 2011; Nagakura et al. 2011). The observations of the spectral peak energy-peak luminosity relation also imply that the GRB formation rate does not significantly decrease to $z \sim 12$ (Yonetoku et al. 2004; Nava et al. 2011).

Observations of such energetic GRBs at very high redshifts will provide a unique probe of the high-redshift Universe (Lamb & Reichart 2000; Ciardi & Loeb 2000; Gou et al. 2004; Yonetoku et al. 2004). Ioka & Mészáros (2005) study the radio

afterglows of high-redshift GRBs and show that they can be observed out to $z \sim 30$ by VLA[1], LOFAR[2], and SKA[3] (see also Ioka 2003). Inoue et al. (2007) calculate time-dependent, broadband afterglow spectra of high-redshift GRBs. They suggest that spectroscopic measurements of molecular and atomic absorption lines due to ambient protostellar gas may be possible to $z \sim 30$ and beyond with ALMA[4], EVLA[5], and SKA. In the future, it will be also promising to observe the GRB afterglows located by gamma-ray satellites such as *Swift*[6], SVOM[7], JANUS[8], and EXIST[9]. Clearly, it is important to study the rate and the detectability of Pop III GRBs at very high redshifts.

There have been already a few observations of GRBs at high redshifts. GRB 090429B at $z = 9.4$ (Cucchiara et al. 2011) is the current record-holding object, followed by a $z = 8.6$ galaxy (Lehnert et al. 2010), GRB 090423 at $z = 8.26$ (Salvaterra et al. 2009; Tanvir et al. 2009), GRB 080913 at $z = 6.7$ (Greiner et al. 2009), GRB 050904 at $z = 6.3$ (Kawai et al. 2006; Totani et al. 2006), and the highest redshift quasars at $z = 7.085$

---

[1] http://www.vla.nrao.edu/

[2] http://www.lofar.org/index.htm

[3] http://www.skatelescope.org/

[4] www.alma.nrao.edu/

[5] http://www.aoc.nrao.edu/evla

[6] http://swift.gsfc.nasa.gov/docs/swift/swiftsc.html

[7] http://www.svom.fr/svom.html

[8] http://sms.msfc.nasa.gov/xenia/pdf/CCE2010/Burrows.pdf

[9] http://exist.gsfc.nasa.gov/design/

(Mortlock et al. 2011) and $z = 6.41$ (Willott et al. 2003). Chandra et al. (2010) report the discovery of radio afterglow emission from GRB 090423 and Frail et al. (2006) for GRB 050904. Observations of afterglows make it possible to derive the physical properties of the explosion and the circumburst medium. It is intriguing to search for these different signatures in the GRB afterglows at low and high redshifts.

The purpose of the present paper is to calculate the Pop III GRB rate detectable by the current and future GRB missions (see also Campisi et al. 2011). We consider high-redshift GRBs of two populations following Bromm et al. (2009). Pop III.1 stars are the first-generation stars that form from initial conditions determined cosmologically. Pop III.2 stars are zero-metallicity stars but formed from a primordial gas that was influenced by earlier generation of stars. Typically, Pop III.2 stars are formed in an initially ionized gas (Johnson & Bromm 2006; Yoshida et al. 2007). The Pop III.2 stars are thought to be less massive ($\sim 40-60\ M_\odot$) than Pop III.1 stars ($\sim 1000\ M_\odot$) but still massive enough for producing GRBs.

We have calculated the GRB rate for these two populations separately for the first time. The rest of the paper is organized as follows. In Sect. 2, we describe a semi-analytical model to calculate the formation rate of primordial GRBs. In Sect. 3, we show our model predictions and calculate the detectability of Pop III GRBs by future satellite missions and by radio observations. In Sect. 4, we discuss the results and give our concluding remarks. Throughout the paper we adopt the standard Λ cold dark matter model with the best fit cosmological parameters from Jarosik et al. (2011) (WMAP-Yr7[10]), $\Omega_m = 0.267, \Omega_\Lambda = 0.734$, and $H_0 = 71$ km s^{-1} Mpc^{-1}.

2. Gamma-ray burst rate

We assume that the formation rate of GRBs is proportional to the star formation rate (Totani 1997; Ishida et al. 2011). The number of observable GRBs per comoving volume per time is expressed as

$$\Psi_{GRB}^{obs}(z) = \frac{\Omega_{obs}}{4\pi} \eta_{GRB}\, \eta_{beam}\, \Psi_*(z) \int_{\log L_{lim}(z)}^{\infty} p(L) d\log L, \qquad (1)$$

where η_{GRB} is the GRB formation efficiency (see Sect. 2.6), η_{beam} the beaming factor of the burst, Ω_{obs} the field of view of the experiment, Ψ_* the cosmic star formation rate (SFR) density, and $p(L)$ the GRB luminosity function in X-rays to gamma rays. The intrinsic GRB rate is given by

$$\Psi_{GRB}(z) = \eta_{GRB}\Psi_*(z). \qquad (2)$$

The quantity $L_{lim}(z)$ is the minimum luminosity threshold to be detected, which is specified for a given experiment. The non-isotropic nature of GRBs gives $\eta_{beam} \sim 0.01-0.02$ (Guetta et al. 2005). Using a radio transient survey, Gal-Yam et al. (2006) place an upper limit of $\eta_{beam} \lesssim 0.016$. Given the average value of jet opening angle $\theta \sim 6°$ (Ghirlanda et al. 2007) and $\eta_{beam} \sim 5.5 \times 10^{-3}$, we set $\eta_{beam} = 0.006$ as a fiducial value. The adopted values of Ω_{obs} are 1.4, 2, 4, and 5 for *Swift*, SVOM, JANUS, and EXIST, respectively (Salvaterra et al. 2008).

2.1. The number of collapsed objects

We first calculate the star formation rate (SFR) at early epochs. Assuming that stars are formed in collapsed dark matter halos,

we follow a popular prescription in which the number of collapsed objects is calculated by the halo mass function (Hernquist & Springel 2003; Greif & Bromm 2006; Trenti & Stiavelli 2009). We adopt the Sheth-Tormen mass function, f_{ST}, (Sheth & Tormen 1999) to estimate the number of dark matter halos, $n_{ST}(M, z)$, with mass less than M per comoving volume at a given redshift:

$$f_{ST} = A \sqrt{\frac{2a_1}{\pi}} \left[1 + \left(\frac{\sigma^2}{a_1 \delta_c^2}\right)^p\right] \frac{\delta_c}{\sigma} \exp\left[-\frac{a_1 \delta_c^2}{2\sigma^2}\right], \qquad (3)$$

where $A = 0.3222, a_1 = 0.707, p = 0.3$ and $\delta_c = 1.686$. The mass function f_{ST} can be related to the $n_{ST}(M, z)$ as

$$f_{ST} = \frac{M}{\rho_m} \frac{dn_{ST}(M, z)}{d \ln \sigma^{-1}}, \qquad (4)$$

where ρ_m is the total mass density of the background Universe. The variance of the linear density field $\sigma(M, z)$ is given by

$$\sigma^2(M, z) = \frac{b^2(z)}{2\pi^2} \int_0^\infty k^2 P(k) W^2(k, M) dk, \qquad (5)$$

where $b(z)$ is the growth factor of linear perturbations normalized to $b = 1$ at the present epoch, and $W(k, M)$ is the Fourier-space top hat filter. To calculate the power spectrum $P(k)$, we use the CAMB code[11] for our assumed ΛCDM cosmology.

2.2. H_2 photodissociation

The star formation efficiency in the early Universe largely depends on the ability of a primordial gas to cool and condense. Hydrogen molecules (H_2) are the primary coolant in a gas in small mass "minihalos", and are also fragile to soft ultraviolet radiation, and thus a ultraviolet background in the Lyman-Werner (LW) bands can easily suppress the star formation inside minihalos. We model the dissociation effect by setting the minimum mass for halos that are able to host Pop III stars (Yoshida et al. 2003).

For the minimum halo mass capable of cooling by molecular hydrogen in the presence of a Lyman-Werner (LW) background, we adopt a fitting formula given by Machacek et al. (2001) and Wise & Abel (2005), which also agrees with results from O'Shea & Norman (2008):

$$M_{H_2} = \exp\left(\frac{f_{cd}}{0.06}\right) \left(1.25 \times 10^5 + 8.7 \times 10^5 F_{LW,-21}^{0.47}\right), \qquad (6)$$

where $F_{LW,-21} = 4\pi J_{LW}$ is the flux in the LW band in units of 10^{-21} erg^{-1} s^{-1} cm^{-2} Hz^{-1}, and f_{cd} the fraction of gas that is cold and dense. We set $f_{cd} = 0.02$ as a conservative estimate. We compute the LW flux consistently with the comoving density in stars $\rho_*(z)$ via a conversion efficiency η_{LW} (Greif & Bromm 2006):

$$J_{LW} = \frac{hc}{4\pi m_H} \eta_{LW} \rho_*(z)(1 + z)^3. \qquad (7)$$

Here, η_{LW} is the number of photons emitted in the LW bands per stellar baryon and m_H is the mass of hydrogen. The value of η_{LW} depends on the characteristic mass of the formed primordial stars, but the variation is not very large for stars with masses greater than ten solar masses (Schaerer 2002). We set $\eta_{LW} = 10^4$ for both Pop III.1 and Pop III.2 for simplicity.

Next we calculate the stellar mass density as

$$\rho_*(z) = \int \Psi_*(z') \left| \frac{dt}{dz'} \right| dz'. \tag{8}$$

For a given z, the integral is performed over the maximum distance that an LW photon can travel before it is redshifted out of the LW bands. The mean free path of LW photons at $z = 30$ is $\sim$10 Mpc (physical). Photons travel over the mean free path in $\sim 10^7$ yr (Mackey et al. 2003). Halos with virial temperature less than 10^4 Kelvin cool almost exclusively by H_2 line cooling, and produce mostly massive stars. We adopt the mass of such halos, $M(T_{vir} = 10^4$ K, $z)$, as an upper limit of halos that produce Pop III.1 stars. In larger halos, the gas is ionized at virialization, and thus the formed stars have, according to our definition, similar properties to Pop III.2 stars. We assume that $M(T_{vir} = 10^4$ K, $z)$ is the minimum halo mass for Pop III.2 star formation.

The collapsed fraction of mass, $F_{col}(z)$, available for Pop III star formation is given by

$$F_{col}^{III.1}(z) = \frac{1}{\rho_m} \int_{M_{H_2}}^{M_{T_{vir}=10^4 K}} dM M n_{ST}(M, z) \tag{9}$$

for Pop III.1 stars, and

$$F_{col}^{III.2}(z) = \frac{1}{\rho_m} \int_{M_{T_{vir}=10^4 K}}^{\infty} dM M n_{ST}(M, z) \tag{10}$$

for Pop III.2. Using the above criteria, the SFR of Pop III stars can be written as

$$\Psi_*^{III.1}(z) = (1 - Q_{HII}(z))(1 - \zeta(z, v_{wind}))\rho_m f_b f_* \frac{dF_{col}^{III.1}}{dt} \tag{11}$$

for Pop III.1 stars, and

$$\Psi_*^{III.2}(z) = Q_{HII}(z)(1 - \zeta(z, v_{wind}))\rho_m f_b f_* \frac{dF_{col}^{III.2}}{dt} \tag{12}$$

for Pop III.2. Here, $\zeta(z, v_{wind})$ represents the global filling fraction of metals via galactic winds (see Sect. 2.4), $Q_{HII}(z)$ the volume filling fraction of ionized regions (see Sect. 2.3), and f_b is the baryonic mass fraction. For the star formation efficiency, we use the value $f_* = 0.001$ as a conservative choice (Greif & Bromm 2006) and $f_* = 0.1$ (Bromm & Loeb 2006) as an upper limit. The latter choice is not strictly consistent with the assumption made in Eq. (6). We explore a model with $f_* = 0.1$ simply to show a very optimistic case.
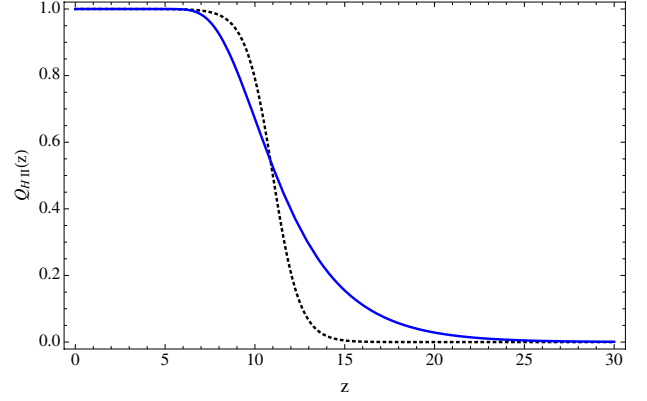
2.3. Reionization

Inside growing HII regions, the gas is highly ionized, and the temperature is $\sim 10^4$ K, so the formation of Pop III.1 stars is terminated according to our definition. The formation rate of Pop III.1 is reduced by a factor given by the volume filling fraction of ionized regions, $Q_{HII}(z)$. We follow Wyithe & Loeb (2003) to calculate the evolution of $Q_{HII}(z)$ as

$$\frac{dQ_{HII}}{dz} = \frac{N_{ion}}{0.76} \frac{dF_{col}}{dt} - \alpha_B \frac{C}{a^3} n_H^0 Q_{HII}, \tag{13}$$

whose solution is

$$Q_{HII}(z) = \int_z^{\infty} dz' \frac{dt}{dz'} \frac{N_{ion}}{0.76} \frac{dF_{col}}{dt} e^{F(z',z)}, \tag{14}$$

Fig. 1. Reionization history calculated using our model. The blue line is our model prediction, and the dotted black line is the best fit of CAMB code.

where

$$F(z', z) = -\frac{2}{3} \frac{\alpha_B n_H^0}{\sqrt{\Omega_m} H_0} C[f(z') - f(z)], \tag{15}$$

and

$$f(z) = \sqrt{(1 + z)^3 + \frac{1 - \Omega_m}{\Omega_m}}. \tag{16}$$

Here we have assumed the primordial fraction of hydrogen of 0.76. In the above equations, $N_{ion} \equiv N_\gamma f_* f_{esc}$ is an efficiency parameter that gives the number of ionizing photons per baryon, where f_{esc} is the fraction of ionizing photons able to escape the host galaxy, and N_γ is the time averaged number of ionizing photons emitted per unit stellar mass formed. The quantity $n_H^0 = 1.95 \times 10^{-7}$ cm^{-3} is the present-day comoving number density of hydrogen, $\alpha_B = 2.6 \times 10^{-13}$ cm^3 s^{-1} is the hydrogen recombination rate, and $C = \langle n_H^2 \rangle / \bar{n}_H^2$ the clumping factor. We use the average value $C = 4$ (see Pawlik et al. 2009 for detailed discussion about redshift dependence of C). We set the values $f_{esc} = 0.7$, $f_* = 0.01$, and $N_\gamma = 9 \times 10^4$ as fiducial values (Greif & Bromm 2006).

In Fig. 1 we show the reionization history calculated using our model in comparison with a fitting function that is the default parametrization of reionization in CAMB (Lewis et al. 2000).

2.4. Metal enrichment

We need to consider metal enrichment in the intergalactic medium (IGM) in order to determine when the formation of primordial stars is terminated (locally) and when the star formation switches from the Pop III mode to a more conventional one.

It is thought that Pop III stars do not generate strong stellar winds, and thus the main contribution to the metal pollution comes from their supernova explosions. Madau et al. (2001) argue that pregalactic outflows from the same primordial halos that reionize the IGM could also pollute it with a substantial amount of heavy elements. To incorporate the effect of metal enrichment by galactic winds, we adopt a similar prescription to Johnson (2010) and Furlanetto & Loeb (2005).

We assume that star-forming halos ("galaxies") launch a wind of metal-enriched gas at $z_* \sim 20$. The metal-enriched wind propagates outward from a central galaxy with a velocity v_{wind},
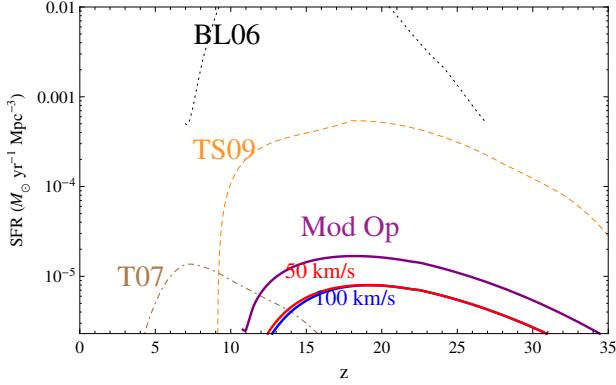
Fig. 2. Pop III.1 star formation rate. Calculated for weak and strong chemical feedback models and a moderate star formation efficiency with $f_* = 0.05$. The results are shown for $v_{wind} = 50$ km s^{-1} , red line; and 100 km s^{-1}, blue line. We also show the theoretical SFRs in the literature, from Bromm & Loeb (2006) (Pop III.1+III.2), dotted black line; Trenti & Stiavelli (2009) (Pop III.2), dashed orange line; and Tornatore et al. (2007) (Pop III.1+III.2), dot-dashed brown line. The purple line is our optimistic model where we assume a very high star formation efficiency, $f_* \sim 0.1$, and low chemical enrichment, $v_{wind} = 50$ km s^{-1}.
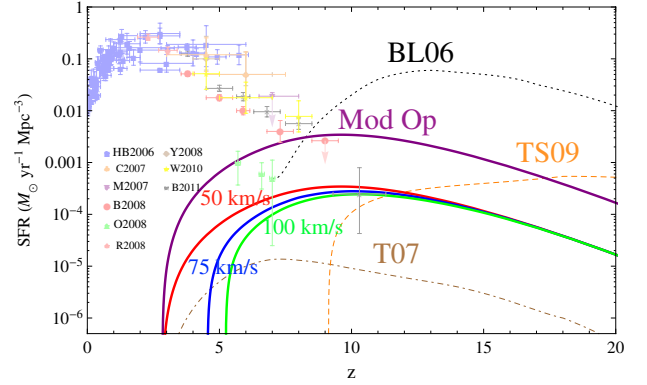
Fig. 3. Pop III.2 star formation rate. Calculated for three different chemical feedback models; $v_{wind} = 50$ km s^{-1}, red line; $v_{wind} = 75$ km s^{-1}, blue line; and $v_{wind} = 100$ km s^{-1}, green line. We also show the theoretical SFRs in the literature, from Bromm & Loeb (2006) (Pop III.1+III.2), dotted black line; Trenti & Stiavelli (2009) (Pop III.2), dashed orange line; and Tornatore et al. (2007) (Pop III.1+III.2), dot-dashed brown line. The purple line is our optimistic model where we assume a very high star formation efficiency, $f_* \sim 0.01$, and low chemical enrichment, $v_{wind} = 50$ km s^{-1}. The light points are independent SFR determinations compiled from the literature.

traveling over a comoving distance R_{wind} given by

$$R_{wind} = \int_{z_*}^{z} v_{wind}(1 + z') \frac{dt}{dz'} dz'. \tag{17}$$

Then we can express f_{chem}, the ratio of gas mass enriched by the wind to the total gas mass in each halo, as

$$f_{chem}(M, z, v_{wind}) = \frac{4\pi}{3} \frac{R_{wind}^3}{V_H}, \tag{18}$$

where $V_H \propto R_H^3$ is the volume of each halo. The halo radius R_H can be approximated by

$$R_H(M) = \left(\frac{3M}{4\pi \times 180\rho_m} \right)^{1/3}. \tag{19}$$

Equation (18) takes the self-enrichment of each halo into account. The next step is to evaluate the average metallicity over cosmic scales. The fraction of cosmic volume enriched by the winds can then be written as

$$\zeta(z, v_{wind}) = \frac{1}{\rho_m} \int dM f_b f_* f_{chem}(M, z, v_{wind}) M n_{ST}(M, z). \tag{20}$$

Although this may appear a significant oversimplification, the model with v_{wind} as a single parameter indeed provides good insight into the impact of the metal enrichment.

We adopt three different values of v_{wind} and examine the effect of metal enrichment quantitatively. We assume that Pop III stars are not formed in a metal-enriched region, regardless of the actual metallicity. Even a single pair instability supernova can enrich the gas within a small halo to a metallicity level well above the critical metallicity (see e.g. Schneider et al. 2006). We effectively assume that the so-called critical metallicity is very low (Schneider et al. 2002, 2003; Bromm & Loeb 2003; Omukai et al. 2005; Frebel et al. 2007; Belczynski et al. 2010).

Figures 2 and 3 show the star formation rate (SFR) history for both Pop III.1 and Pop III.2 considering three different values of the galactic wind, $v_{wind} = 50, 75, 100$ km s^{-1}. Figure 2 shows that the metal enrichment has little influence on Pop III.1. This is

because Pop III.1 formation is terminated early due reionization. In Fig. 3 we compare the Pop III.2 SFR history with a compilation of independent measures from Hopkins & Beacom (2006) up to $z \approx 6$ and from observations of color-selected Lyman break galaxies (Mannucci et al. 2007; Bouwens et al. 2008, 2011), Lyα Emitters (Ota et al. 2008), UV+IR measurements (Reddy et al. 2008), and GRB observations (Chary et al. 2007; Yüksel et al. 2008; Wang & Dai 2009) at higher z (hereafter, these will be referred to as H2006, M2007, B2008, B2011, O2008, R2008, C2007, Y2008, and W2009, respectively). The optimistic case for Pop III.2 is chosen to keep the SFR always below the observationally determined SFR at $z < 8$.

We compared our model results with the SFRs estimated by other authors in the literature Bromm & Loeb (2006), Tornatore et al. (2007), Trenti & Stiavelli (2009), and also see Naoz & Bromberg (2007). It is important to note that Pop III formation can continue to low redshifts ($z < 10$) depending on the level of metal enrichment. Tornatore et al. (2007) use cosmological simulations to show that, because of limited efficiency of heavy element transport by outflows, Pop III star formation continues to form down to $z = 2.5$ (which intriguingly matches our model with $v_{wind} = 50$ km s^{-1} in Fig. 3). The SFR of Tornatore et al. (2007) has a peak value of 10^{-5} $M_\odot$ yr^{-1} Mpc^{-3} at $z \approx 6$.

In Fig. 4 we also show the result of our model with $f_* = 0.1$–0.01 and $v_{wind} = 50$ km s^{-1} for both Pop III.1 and Pop III.2, respectively. This model provides an "optimistic" estimate for the detectable GRB rate for the future missions (see Sect. 3).

2.5. Luminosity function

The number of GRBs detectable by any given instrument depends on the instrument-specific flux sensitivity threshold and also on the intrinsic isotropic luminosity function of GRBs. For the latter, we adopt the power-law distribution function of Wanderman & Piran (2010)

$$p(L) = \begin{cases} \left(\frac{L}{L_*} \right)^{-0.2^{+0.2}_{-0.1}} & L < L_*, \\ \left(\frac{L}{L_*} \right)^{-1.4^{+0.3}_{-0.6}} & L > L_*, \end{cases} \tag{21}$$
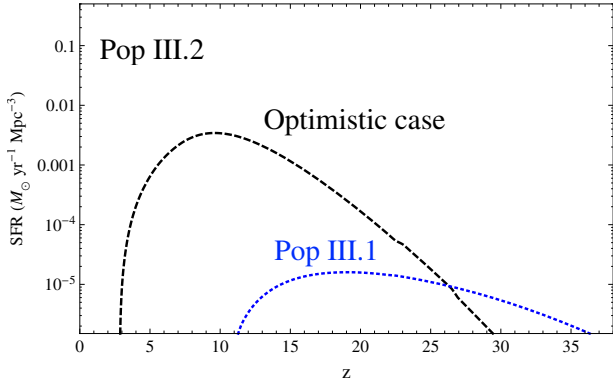
Fig. 4. Comparison of the star formation rates for Pop III.1 (blue dotted line) and for Pop III.2 (dashed black line), for our optimistic model with a high star formation efficiency $f_* = 0.1$ for Pop III.1, $f_* = 0.01$ for Pop III.2 and slow chemical enrichment $v_{\rm wind} = 50$ km s^{-1}.

where L_* is the characteristic isotropic luminosity. We set $L_* \sim 10^{53}$ erg/s for Pop III.1, whereas $L_* \sim 10^{52}$ erg/s for Pop III.2 stars are similar to ordinary GRBs (Li 2008; Wanderman & Piran 2010). The Pop III.1 GRBs are assumed to be energetic with isotropic kinetic energy $E_{\rm iso} \sim 10^{56-57}$ erg but long-lived $T_{90} \sim 1000$ s, so that the luminosity would be moderate $L_* \sim \epsilon_\gamma \times 10^{56-57}/1000 \sim 10^{52-53}$ erg/s if $\epsilon_\gamma \sim 0.1$ is the conversion efficiency from the jet kinetic energy to gamma rays (Suwa & Ioka 2011).

Using the above relation we can predict the observable GRB rate for the *Swift*, SVOM, JANUS, and EXIST missions. For *Swift*, we set a bolometric energy flux limit $F_{\rm lim} = 1.2 \times 10^{-8}$ erg cm^{-2} s^{-1} (Li 2008). We adopt a similar limit for SVOM (Paul et al. 2011). For JANUS, $F_{\rm lim} \sim 10^{-8}$ erg cm^{-2} s^{-1} (Falcone et al. 2009). The luminosity threshold is then

$$L_{\rm lim} = 4\pi\, d_{\rm L}^2\, F_{\rm lim}. \tag{22}$$

Here d_L is the luminosity distance for the adopted ΛCDM cosmology. EXIST is expected to be $\sim 7-10$ times more sensitive than *Swift* (Grindlay 2010). We set the EXIST sensitivity threshold to ten times lower than *Swift* as an approximate estimate. For simplicity, we assume that the spectral energy distribution (SED) peaks at X-to-γ ray energy (detector bandwidth) as an optimistic case. The rate would be less if the SED is very different from Pop II/I GRBs.

2.6. Initial mass function and GRB formation efficiency

The stellar initial mass function (IMF) is critically important for determining the Pop III GRB rate. We define the GRB formation efficiency factor per stellar mass as

$$\eta_{\rm GRB} = f_{\rm GRB} \frac{\int_{M_{\rm GRB}}^{M_{\rm up}} \phi(m)\mathrm{d}m}{\int_{M_{\rm low}}^{M_{\rm up}} m\phi(m)\mathrm{d}m}, \tag{23}$$

where $\phi(m)$ is the stellar IMF, and $f_{\rm GRB} = 0.001$ is the GRB fraction, since we expect one GRB every 1000 supernovae (Langer & Norman 2006). We assume that Pop III GRBs have a similar fraction to the standard case. Izzard et al. (2004) argue that GRB formation efficiency could increase by a factor of $5-7$ for low-metallicity stars ($\sim 10^{-2}\, Z_\odot$). If most of the first stars are rotating rapidly as suggested by Stacy et al. (2011), we can expect that a significant fraction of the first stars can produce GRBs. Thus

given the uncertainty in the parameter for free metal stars, we also explore the possibility that $f_{\rm GRB}$ is $10 - 100\times$ higher.

We consider the following two forms of IMF. One is a power law with the standard Salpeter slope

$$\phi(m) \propto m^{-2.35}, \tag{24}$$

and the other is a Gaussian IMF (Scannapieco et al. 2003; Nakamura & Umemura 2001):

$$\phi(m)m^{-1}\,\mathrm{d}m = \frac{1}{\sqrt{2\pi}\sigma_{\rm c}(M)} e^{-(m-\bar{M})^2/2\sigma_{\rm c}(M)^2}\mathrm{d}m. \tag{25}$$

For the latter, we assume $\bar{M} = 550\, M_\odot$ for Pop III.1 and $\bar{M} = 55\, M_\odot$ for Pop III.2, with dispersion $\sigma_c = (\bar{M} - M_{\rm low})/3$. $M_{\rm low}$ is the minimum mass for a given stellar type, $100\, M_\odot$ for Pop III.1, and $10\, M_\odot$ for Pop III.2, whereas $M_{\rm up}$ is the maximum mass for a given stellar type, $1000\, M_\odot$ for Pop III.1, and $\sim 100\, M_\odot$ for Pop III.2. $M_{\rm GRB}$ is the minimum mass that is able to trigger GRBs, which we set to be $25\, M_\odot$ (Bromm & Loeb 2006). Not all Pop III.1 stars will leave a black hole behind at their deaths. In the narrow mass range of $\sim 140-260\, M_\odot$ Pop III stars are predicted to undergo a pair-instability supernova (PISN) explosion (Heger & Woosley 2002). This range of mass is excluded from the calculation of Eq. (23).

The efficiency factor for the power-law (Salpeter) IMF is $\eta_{\rm GRB}/f_{\rm GRB} \sim 1/926\, M_\odot^{-1}$ and $1/87\, M_\odot^{-1}$ for Pop III.1 and Pop III.2, respectively. Using the Gaussian IMF, $\eta_{\rm GRB}/f_{\rm GRB} \sim 1/538\, M_\odot^{-1}$ and $1/53\, M_\odot^{-1}$ for Pop III.1 and Pop III.2. respectively. Thus, the GRB formation efficiency for Pop III.2 can be about an order of magnitude higher than Pop III.1 because of the lower characteristic mass of Pop III.2 stars.

3. Redshift distribution of GRBs

Over a particular time interval, $\Delta t_{\rm obs}$, in the observer rest frame, the number of observed GRBs originating between redshifts z and $z + \mathrm{d}z$ is

$$\frac{\mathrm{d}N_{\rm GRB}^{\rm obs}}{\mathrm{d}z} = \Psi_{\rm GRB}^{\rm obs}(z)\frac{\Delta t_{\rm obs}}{1+z}\frac{\mathrm{d}V}{\mathrm{d}z}, \tag{26}$$

where $\mathrm{d}V/\mathrm{d}z$ is the comoving volume element per unit redshift, given by

$$\frac{\mathrm{d}V}{\mathrm{d}z} = \frac{4\pi c\, d_{\rm L}^2}{(1+z)}\left|\frac{\mathrm{d}t}{\mathrm{d}z}\right|. \tag{27}$$

Figure 5 shows the intrinsic GRB rate

$$\frac{\mathrm{d}N_{\rm GRB}}{\mathrm{d}z} = \Psi_{\rm GRB}(z)\frac{\Delta t_{\rm obs}}{1+z}\frac{\mathrm{d}V}{\mathrm{d}z}. \tag{28}$$

In this plot, we have not considered observational effects such as beaming and instrument sensitivity; namely, we set $\Omega_{\rm obs} = 4\pi, \eta_{\rm beam} = 1$, and $L_{\rm lim}(z) = 0$ in Eq. (1). We show the GRB rate for our choice of two different IMFs. Interestingly, Fig. 5 shows that the results depend only weakly on the choice of IMF.

Figure 6 shows the most optimistic case, assuming a high star formation efficiency $f_* = 0.1$ for Pop III.1, $f_* = 0.01$ for Pop III.2, an inefficient chemical enrichment, $v_{\rm wind} = 50$ km s^{-1}, $f_{\rm GRB} = 0.1$, and a Gaussian IMF for both Pop III.1 and Pop III.2 stars. We note that constraints on these quantities will be useful for placing upper limits on the GRB observed rate.
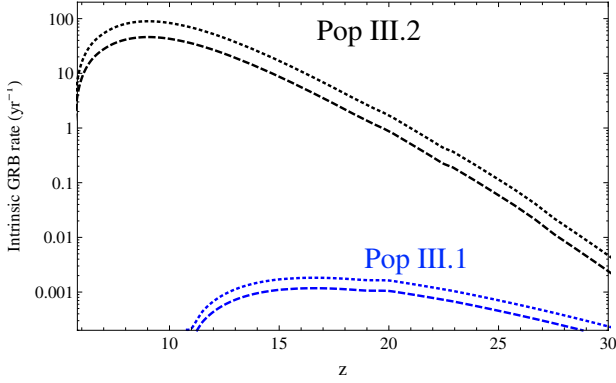
Fig. 5. The intrinsic GRB rate dN_{GRB}/dz. The number of (on-axis + off-axis) GRBs per year on the sky in Eq. (28), as a function of redshift. We set $f_* = 0.001$, $f_{GRB} = 0.01$ and $v_{wind} = 100$ km s^{-1} for this plot. Salpeter IMF, dashed black line, Gaussian IMF, dotted black line, for Pop III.2; and Salpeter IMF, dashed blue line, Gaussian IMF, dotted blue line, for Pop III.1.
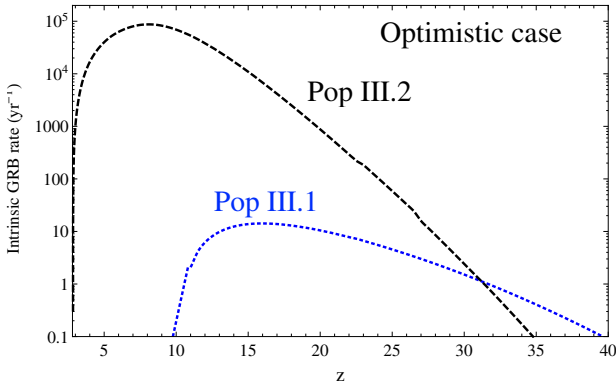
Fig. 6. The intrinsic GRB rate dN_{GRB}/dz. The number of (on-axis + off-axis) GRBs per year on the sky in Eq. (28), as a function of redshift for our optimistic model. We assume a high star formation efficiency; $f_* = 0.1$ for Pop III.1; and $f_* = 0.01$ for Pop III.2; slow chemical enrichment, $v_{wind} = 50$ km s^{-1}; high GRB formation efficiency, $f_{GRB} = 0.1$; and a Gaussian IMF; for both Pop III.2, dashed black line; and Pop III.1, dotted blue line.

3.1. Radio afterglows

Follow-up observations of high-redshift GRBs can be done by observing their afterglows, especially in radio band (Ioka & Mészáros 2005; Inoue et al. 2007). We calculated the radio afterglow light curves for Pop III GRBs following the standard prescription from Sari et al. (1998, 1999) and Mészáros (2006). The afterglow light curve at the time t_d is given by the shock radius r_d and the Lorentz factor γ_d. These two quantities are related by $E_{iso} \sim 4\pi r_d^3 \gamma_d^2 n m_p c^2$ and $r_d \sim c\gamma_d^2 t_d$, where n is the medium density and m_p the proton mass. The true energy is given by $E_{true} = \theta^2 E_{iso}/2$, where θ is the half opening angle of the shock. The spectrum consists of power-law segments linked by critical break frequencies. These are ν_a (the self absorption frequency), ν_m (the peak of injection frequency), and ν_c (the cooling

frequency), given by

$$
\begin{aligned}
\nu_m &\propto (1+z)^{1/2} g(p)^2 \epsilon_e^2 \epsilon_B^{1/2} E_{iso}^{1/2} t_d^{-3/2}, \\
\nu_c &\propto (1+z)^{-1/2} \epsilon_B^{-3/2} n^{-1} E_{iso}^{-1/2} t_d^{-1/2}, \\
\nu_a &\propto (1+z)^{-1} \epsilon_e^{-1} \epsilon_B^{1/5} n^{3/5} E_{iso}^{1/5}, \\
F_{\nu,max} &\propto (1+z) \epsilon_B^{1/2} n^{1/2} E_{iso} d_L^{-2},
\end{aligned} \tag{29}
$$

where $g(p) = (p-2)/(p-1)$ is a function of energy spectrum index of electrons ($N(\gamma_e)d\gamma_e \propto \gamma_e^{-p} d\gamma_e$, where γ_e is the electron Lorentz factor), and ϵ_e and ϵ_B are the efficiency factors (Mészáros 2006). There are two types of spectra. If $\nu_m < \nu_c$, we call it the *slow cooling case*. The flux at the observer, F_ν, is given by

$$
F_\nu = \begin{cases}
(\nu_a/\nu_m)^{1/3}(\nu/\nu_a)^2 F_{\nu,max}, & \nu_a > \nu, \\
(\nu/\nu_m)^{1/3} F_{\nu,max}, & \nu_m > \nu > \nu_a, \\
(\nu/\nu_m)^{-(p-1)/2} F_{\nu,max}, & \nu_c > \nu > \nu_m, \\
(\nu_c/\nu_m)^{-(p-1)/2}(\nu/\nu_c)^{-p/2} F_{\nu,max}, & \nu > \nu_c,
\end{cases} \tag{30}
$$

where $F_{\nu,max}$ is the observed peak flux at distance d_L from the source.

For $\nu_m > \nu_c$, called the fast cooling case, the spectrum is

$$
F_\nu = \begin{cases}
(\nu_a/\nu_c)^{1/3}(\nu/\nu_a)^2 F_{\nu,max}, & \nu_a > \nu, \\
(\nu/\nu_c)^{1/3} F_{\nu,max}, & \nu_c > \nu > \nu_a, \\
(\nu/\nu_c)^{-1/2} F_{\nu,max}, & \nu_m > \nu > \nu_c, \\
(\nu_m/\nu_c)^{-1/2}(\nu/\nu_m)^{-p/2} F_{\nu,max}, & \nu > \nu_m.
\end{cases} \tag{31}
$$

As the GRB jet sweeps the interstellar medium, the Lorentz factor of the jet is decelerated. When the Lorentz factor drops below θ^{-1}, the jet starts to expand sideways and becomes detectable by the off-axis observers. These afterglows are not associated with the prompt GRB emission. Such *orphan* afterglows are a natural consequence of the existence of GRB's jets. Radio transient sources probe the high-energy population of the Universe and can provide further constraints on the intrinsic rate of GRBs. Even if the prompt emission is highly collimated, the Lorentz factor drops $\gamma_d < \theta^{-1}$ around the time

$$
t_\theta \sim 2.14 \left(\frac{E_{iso}}{5 \times 10^{54}}\right)^{1/3} \left(\frac{\theta}{0.1}\right)^{8/3} n^{-1/3}(1+z) \text{ days}, \tag{32}
$$

and the jet starts to expand sideways. Finally the shock velocity becomes nonrelativistic around the time

$$
t_{NR} \sim 1.85 \times 10^2 \left(\frac{E_{iso}}{5 \times 10^{54}}\right)^{1/3} \left(\frac{\theta}{0.1}\right)^{2/3} n^{-1/3}(1+z) \text{ days}, \tag{33}
$$

(Ioka & Mészáros 2005). After time t_θ, the temporal dependence of the critical break frequencies should be replaced by $\nu_c \propto t^0, \nu_m \propto t^{-2}, \nu_a \propto t^{-1/5}$, and $F_{\nu,max} \propto t^{-1}$ (Sari et al. 1999). We also used the same evolution in the nonrelativistic phase for simplicity, which underestimates the afterglow flux after t_{NR}.

Figure 7 shows the light curves for a typical GRB from Pop III.2 stars assuming an isotropic kinetic energy $E_{iso} \sim 10^{54}$ erg (in proportion to the progenitor mass) as a lower limit. Pop III.1 afterglows are expected to be brighter. Consistently with previous works, we conclude that it is possible to observe the GRB radio afterglows with ALMA, LOFAR, EVLA, and SKA.
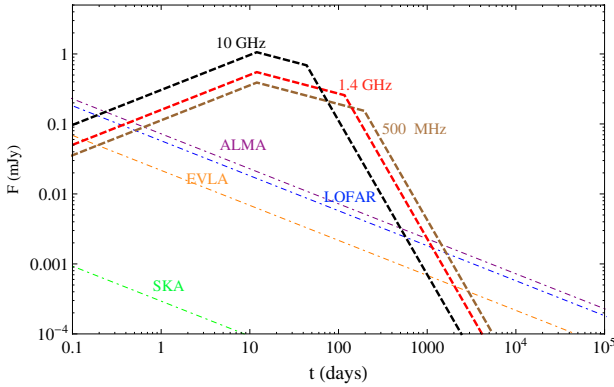
Fig. 7. The theoretical light curve of radio afterglow of a typical Pop III.2 GRB at $z \sim 10$. We show the evolution of afterglow flux F(mJy) as a function of time t (days) for typical parameters: isotropic kinetic energy $E_{iso} = 10^{54}$ erg, electron spectral index $p = 2.5$, plasma parameters $\epsilon_e = 0.1$, $\epsilon_B = 0.01$, initial Lorentz factor $\gamma_d = 200$, interstellar medium density $n = 1$ cm^{-3}, for the range of frequencies: 500 MHz (dashed brown line), 1.4 GHz (dashed red line), 10 GHz (dashed black line), in comparison with flux sensitivity F_ν^{sen} as a function of integration time, t_{int}(days) for SKA (dot-dashed green line), EVLA (dot-dashed orange line), LOFAR (dot-dashed blue line) and ALMA (dot-dashed purple line).

3.2. Upper limits from radio transient survey

In this section, we derive upper limits on the intrinsic GRB rate (including the off-axis GRB) using ~1 year timescale radio variability surveys. There are several radio transient surveys completed so far. Bower et al. (2007) used 22 years of archival data from VLA to put an upper limit of ~6 deg^{-2} for 1-year variability transients above 90 μJy, which is equivalent to $\lesssim 2.4 \times 10^5$ for the whole sky. Gal-Yam et al. (2006) used FIRST[12] and NVSS[13] radio catalogs to place an upper limit of ~70 radio orphan afterglows above 6 mJy in the 1.4 GHz band over the entire sky. This suggests less than 3×10^4 sources above 0.3 mJy on the sky, because the number of sources is expected to be proportional to flux limit $F_{lim}^{-3/2}$ (assuming Euclidian space and no source evolution) (Gal-Yam et al. 2006). From Fig. 7, a typical GRB's radio afterglow with isotropic kinetic energy $E_{iso} \sim 10^{54}$ erg stays above 0.3 mJy over ~10^2 days.

By combining the results shown in Figs. 5 and 6, we expect ~$30 - 3 \times 10^5$ sources ($10^2 - 10^6$ events per year × 10^2 days) above ~0.3 mJy. (We integrate the event rate over redshift.) As a consequence, the most optimistic case for Pop III.2 should already be ruled out marginally by the current observations of radio transient sources, if their luminosity function follows the one assumed in the present paper. Only more conservative models are then viable. Radio transient surveys are not yet able to set upper limits on the Pop III.1 GRB rate. The above conclusion is model dependent, because the afterglow flux depends on the still uncertain quantities, such as the isotropic energy E_{iso} and the ambient density n. If the circumburst density is higher than usual, the constraints from the radio transient surveys would be even stronger. Also the GRB formation efficiency and the beaming factor are not known accurately, which can affect both the intrinsic and observed rate more than one order of magnitude.

---

[12] http://sundog.stsci.edu/
[13] http://www.cv.nrao.edu/nvss/
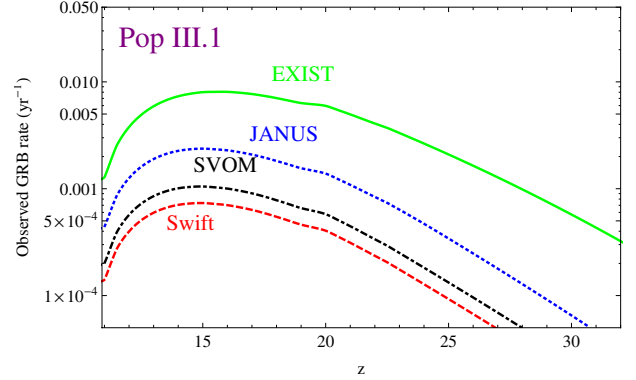
Fig. 8. Predicted Pop III.1 observed GRB rate. Those observed by *Swift*, dashed red line; SVOM, dot-dashed black line; JANUS, dotted blue line; and EXIST, green line. We adopt a GRB rate model that is consistent with the current upper limits from the radio transients; Gaussian IMF, $v_{wind} = 50$ km s^{-1}, $f_* = 0.1$, $f_{GRB} = 0.1$.
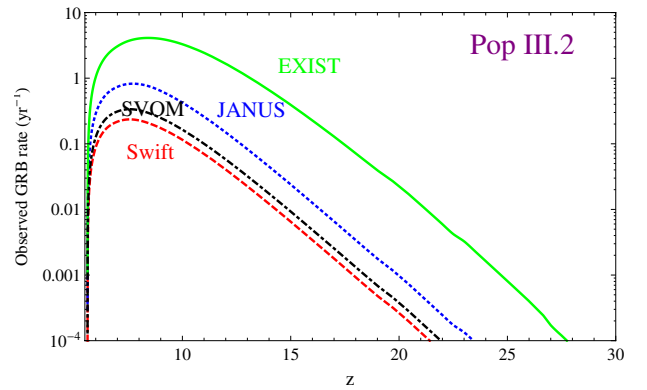
Fig. 9. Predicted Pop III.2 observed GRB rate. Those observed by *Swift*, dashed red line; SVOM, dot-dashed black line; JANUS, dotted blue line; and EXIST, green line; for our model with Salpeter IMF, $v_{wind} = 100$ km s^{-1}, $f_* = 0.01$, $f_{GRB} = 0.01$.

In Figs. 8 and 9, we show the predicted observable GRB rate dN_{GRB}^{obs}/dz in Eq. (26) for Pop III.1 and III.2 detectable by the *Swift*, SVOM, JANUS, and EXIST missions. The results shown are still within the bounds of available upper limits from the radio transient surveys. Overall, it is more likely to observe Pop III.2 GRBs than Pop III.1, but the predicted rate strongly depends on the IGM metallicity evolution, the star formation efficiency and GRB formation efficiency. The dependence on the IMF is relatively small.

Figure 10 shows the GRB rate expected for EXIST observations. Because the power index of the LF is uncertain at the bright end, we added two lines to show the resulting uncertainty in our prediction. We use the maximum rate, which is within the constraints by the current observations of radio transients. We expect to observe $N \sim 20$ GRBs per year at $z > 6$ for Pop III.2 and $N \sim 0.08$ per year for Pop III.1 at $z > 10$ with the future EXIST satellite at a maximum. Our optimist case predicts a near-future detection of Pop III.2 GRB by *Swift*, and the nondetection so far could suggest a further upper limit or difference between the Pop III and present-day GRB spectrum.
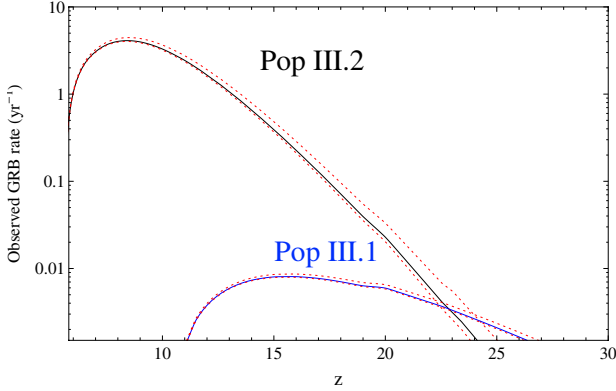
Fig. 10. Predicted maximum GRB rates observed by EXIST. We adopted Salpeter IMF, $v_{wind} = 100$ km s^{-1}, $f_{GRB} = 0.01$, $f_* = 0.01$; for Pop III.2 GRBs, dashed black line; and Gaussian IMF, $v_{wind} = 50$ km s^{-1}, $f_* = 0.1$, $f_{GRB} = 0.1$; for Pop III.1 GRBs, dotted blue line. Dotted red lines represent the same with LF's bright end power law index 1.7 and 0.8.

4. Conclusion and discussion

There are still no direct observations of Population III stars, despite much recent development in theoretical studies on the formation of the early generation stars. In this paper, we follow a recent suggestion that massive Pop III stars could trigger collapsar gamma-ray bursts. Observations of such energetic GRBs at very high redshifts will be a unique probe of the high-redshift Universe. With a semi-analytical approach we estimated the star formation rate for Pop III.1 and III.2 stars including all relevant feedback effects: photo-dissociation, reionization, and metal enrichment.

Using radio transient sources we are able to derive constraints on the intrinsic rate of GRBs. We estimated the predicted GRB rate for both Pop III.1 and Pop III.2 stars, and argued that the latter is more likely to be observed with future experiments. We expect to observe maximum of $N \lesssim 20$ GRBs per year integrated over at $z > 6$ for Pop III.2 and $N \lesssim 0.08$ per year integrated over at $z > 10$ for Pop III.1 with EXIST.

We also expect a larger number of radio afterglows than X-ray prompt emission because the radio afterglow is long-lived, for $\sim 10^2$ days above ~ 0.3 mJy from Fig. 7. Combining with the intrinsic GRB rate and constraints from radio transients, we expect roughly $\sim 10-10^4$ radio afterglows above $\gtrsim 0.3$ mJy already on the sky. They are indeed detectable by ALMA, EVLA, LOFAR, and SKA, and have even been detected already by ~ 1 yr-timescale variability surveys. We showed that using a semi-analytical approach combined with the current surveys, such as NVSS and FIRST, we are already able to constrain the Pop III.2 GRB event rate.

Finally, it is important to note that our knowledge of the first stars and GRBs is still limited, and there are uncertainties in their properties, most significantly in their characteristic mass. Recently, Clark et al. (2011) and Greif et al. (2011) have performed cosmological simulations using a sink particle technique to follow the evolution of a primordial protostellar accretion disk. They find that the disk gravitationally fragments to yield multiple protostellar seeds. Although the final mass distribution of the formed stars is still uncertain, formation of multiple systems, especially massive binary Pop III stars, would increase the rate of high-redshift GRBs (e.g., Bromm & Loeb 2006; Fryer & Heger 2005, and references therein). If the GRB fraction per collapse f_{GRB} in Eq. (23) is much larger than the current one,

say $f_{GRB} \sim 1$, the Pop III.1 GRBs might also become detectable with the radio telescopes (~ 300 afterglows above ~ 0.3 mJy on the sky) and the X-ray satellites (~ 1 event per year for EXIST) in the future.

References

Abel, T., Bryan, G. L., & Norman, M. L. 2002, Science, 295, 93
Barkov, M. V. 2010, Astrophys. Bull., 65, 217
Belczynski, K., Holz, D. E., Fryer, C. L., et al. 2010, ApJ, 708, 117
Bouwens, R. J., Illingworth, G. D., Franx, M., & Ford, H. 2008, ApJ, 686, 230
Bouwens, R. J., Illingworth, G. D., Labbe, I., et al. 2011, Nature, 469, 504
Bower, G. C., Saul, D., Bloom, J. S., et al. 2007, ApJ, 666, 346
Bromm, V., & Loeb, A. 2003, Nature, 425, 812
Bromm, V., & Loeb, A. 2006, ApJ, 642, 382
Bromm, V., Yoshida, N., Hernquist, L., & McKee, C. F. 2009, Nature, 459, 49
Campisi, M. A., Maio, U., Salvaterra, R., & Ciardi, B. 2011, MNRAS, submitted [arXiv:1106.1439]
Chandra, P., Frail, D. A., Fox, D., et al. 2010, ApJ, 712, L31
Chary, R., Berger, E., & Cowie, L. 2007, ApJ, 671, 272
Ciardi, B., & Loeb, A. 2000, ApJ, 540, 687
Clark, P. C., Glover, S. C. O., Smith, R. J., et al. 2011, Science, 331, 1040
Cucchiara, A., Levan, A. J., Fox, D. B., et al. 2011, ApJ, 736, 7
Falcone, A. D., Burrows, D. N., Barthelmy, S., et al. 2009, SPIE Conf. Ser., 7435
Frail, D. A., Cameron, P. B., Kasliwal, M., et al. 2006, ApJ, 646, L99
Frebel, A., Johnson, J. L., & Bromm, V. 2007, MNRAS, 380, L40
Fryer, C. L., & Heger, A. 2005, ApJ, 623, 302
Furlanetto, S. R., & Loeb, A. 2005, ApJ, 634, 1
Gal-Yam, A., Ofek, E. O., Poznanski, D., et al. 2006, ApJ, 639, 331
Ghirlanda, G., Nava, L., Ghisellini, G., & Firmani, C. 2007, A&A, 466, 127
Gou, L. J., Mészáros, P., Abel, T., & Zhang, B. 2004, ApJ, 604, 508
Greif, T. H., & Bromm, V. 2006, MNRAS, 373, 128
Greif, T., Springel, V., White, S., et al. 2011, ApJ, 737, 75
Greiner, J., Krühler, T., Fynbo, J. P. U., et al. 2009, ApJ, 693, 1610
Grindlay, J. E. 2010, in AIP Conf. Ser. 1279, ed. N. Kawai, & S. Nagataki, 212
Guetta, D., Piran, T., & Waxman, E. 2005, ApJ, 619, 412
Heger, A., & Woosley, S. E. 2002, ApJ, 567, 532
Hernquist, L., & Springel, V. 2003, MNRAS, 341, 1253
Hopkins, A. M., & Beacom, J. F. 2006, ApJ, 651, 142
Inoue, S., Omukai, K., & Ciardi, B. 2007, MNRAS, 380, 1715
Ioka, K. 2003, ApJ, 598, L79
Ioka, K., & Mészáros, P. 2005, ApJ, 619, 684
Ishida, E. E. O., de Souza, R. S., & Ferrara, A. 2011, MNRAS, accepted [arXiv:1106.1745]
Izzard, R. G., Ramirez-Ruiz, E., & Tout, C. A. 2004, MNRAS, 348, 1215
Jarosik, N., Bennett, C. L., Dunkley, J., et al. 2011, ApJS, 192, 14
Johnson, J. L. 2010, MNRAS, 404, 1425
Johnson, J. L., & Bromm, V. 2006, MNRAS, 366, 247
Kawai, N., Kosugi, G., Aoki, K., et al. 2006, Nature, 440, 184
Komissarov, S. S., & Barkov, M. V. 2010, MNRAS, 402, L25
Lamb, D. Q., & Reichart, D. E. 2000, ApJ, 536, 1
Langer, N., & Norman, C. A. 2006, ApJ, 638, L63
Lehnert, M. D., Nesvadba, N. P. H., Cuby, J., et al. 2010, Nature, 467, 940
Lewis, A., Challinor, A., & Lasenby, A. 2000, ApJ, 538, 473
Li, L. 2008, MNRAS, 388, 1487
Machacek, M. E., Bryan, G. L., & Abel, T. 2001, ApJ, 548, 509
Mackey, J., Bromm, V., & Hernquist, L. 2003, ApJ, 586, 1
Madau, P., Ferrara, A., & Rees, M. J. 2001, ApJ, 555, 92
Mannucci, F., Buttery, H., Maiolino, R., Marconi, A., & Pozzetti, L. 2007, A&A, 461, 423
Mészáros, P. 2006, Reports on Progress in Physics, 69, 2259
Mészáros, P., & Rees, M. J. 2010, ApJ, 715, 967
Mortlock, D. J., Warren, S. J., Venemans, B. P., et al. 2011, Nature, 474, 616
Nagakura, H., Suwa, Y., & Ioka, K. 2011, ApJ, submitted [arXiv:1104.5691]

Nakamura, F., & Umemura, M. 2001, ApJ, 548, 19

Naoz, S., & Bromberg, O. 2007, MNRAS, 380, 757

Nava, L., Ghirlanda, G., Ghisellini, G., & Celotti, A. 2011, MNRAS, 932

Omukai, K., & Palla, F. 2003, ApJ, 589, 677

Omukai, K., Tsuribe, T., Schneider, R., & Ferrara, A. 2005, ApJ, 626, 627

O'Shea, B. W., & Norman, M. L. 2008, ApJ, 673, 14

Ota, K., Iye, M., Kashikawa, N., et al. 2008, ApJ, 677, 12

Paul, J., Wei, J., Basa, S., & Zhang, S.-N. 2011, C. R. Phys., 12, 298

Pawlik, A. H., Schaye, J., & van Scherpenzeel, E. 2009, MNRAS, 394, 1812

Reddy, N. A., Steidel, C. C., Pettini, M., et al. 2008, ApJS, 175, 48

Salvaterra, R., Campana, S., Chincarini, G., Covino, S., & Tagliaferri, G. 2008, MNRAS, 385, 189

Salvaterra, R., Della Valle, M., Campana, S., et al. 2009, Nature, 461, 1258

Sari, R., Piran, T., & Narayan, R. 1998, ApJ, 497, L17

Sari, R., Piran, T., & Halpern, J. P. 1999, ApJ, 519, L17

Scannapieco, E., Schneider, R., & Ferrara, A. 2003, ApJ, 589, 35

Schaerer, D. 2002, A&A, 382, 28

Schneider, R., Ferrara, A., Natarajan, P., & Omukai, K. 2002, ApJ, 571, 30

Schneider, R., Ferrara, A., Salvaterra, R., Omukai, K., & Bromm, V. 2003, Nature, 422, 869

Schneider, R., Salvaterra, R., Ferrara, A., & Ciardi, B. 2006, MNRAS, 369, 825

Sheth, R. K., & Tormen, G. 1999, MNRAS, 308, 119

Stacy, A., Bromm, V., & Loeb, A. 2011, MNRAS, 413, 543

Suwa, Y., & Ioka, K. 2011, ApJ, 726, 107

Tanvir, N. R., Fox, D. B., Levan, A. J., et al. 2009, Nature, 461, 1254

Toma, K., Sakamoto, T., & Mészáros, P. 2011, ApJ, 731, 127

Tornatore, L., Ferrara, A., & Schneider, R. 2007, MNRAS, 382, 945

Totani, T. 1997, ApJ, 486, L71

Totani, T., Kawai, N., Kosugi, G., et al. 2006, PASJ, 58, 485

Trenti, M., & Stiavelli, M. 2009, ApJ, 694, 879

Wanderman, D., & Piran, T. 2010, MNRAS, 406, 1944

Wang, F. Y., & Dai, Z. G. 2009, MNRAS, 400, L10

Willott, C. J., McLure, R. J., & Jarvis, M. J. 2003, ApJ, 587, L15

Wise, J. H., & Abel, T. 2005, ApJ, 629, 615

Wyithe, J. S. B., & Loeb, A. 2003, ApJ, 586, 693

Yonetoku, D., Murakami, T., Nakamura, T., et al. 2004, ApJ, 609, 935

Yoshida, N., Abel, T., Hernquist, L., & Sugiyama, N. 2003, ApJ, 592, 645

Yoshida, N., Omukai, K., Hernquist, L., & Abel, T. 2006, ApJ, 652, 6

Yoshida, N., Oh, S. P., Kitayama, T., & Hernquist, L. 2007, ApJ, 663, 687

Yüksel, H., Kistler, M. D., Beacom, J. F., & Hopkins, A. M. 2008, ApJ, 683, L5